Swirl Arc: A Model for Swirling, Turbulent, Radiative Arc Heater Flowfields

J. F. Shaeffer*
McDonnell Douglas Corporation, St. Louis, Mo.

A model for swirling, turbulent, radiative arc heater flowfields, typical of those used for ablative testing of materials, is developed. Included in the model are provisions for secondary gas injection with swirl. The model is based on: swirl number less than unity, i.e., no reverse flow in the constrictor; a Prandtl mixing length turbulence formulation; and a gray gas radiation formulation so that absorption near the wall can be included. The resulting time-averaged conservation equations are then solved numerically using a finite-difference technique. The code results predict swirl decay and its influence on arc stability, the global performance parameters such as voltage, bulk enthalpy, and heat flux, and the enthalpy and velocity flowfields. Stability parameters are outlined and included in the arc heated flowfield model. These parameters are the electrical resistance between centerline and wall and the balance between the destabilizing arc column kink forces (expression given) and the swirl stabilizing pressure forces. The resulting flowfield model is used to predict the characteristics of a high-pressure (10-MPa inlet chamber pressure) air arc heater. Progressing axially, i.e., in the direction of the gas gaining energy, these results indicate that: 1) the central enthalpy peak decreases; 2) the swirl flowfield and resultant stabilizing radial force decay rapidly until augmented by secondary wall injection; 3) the radial pressure differential is small, $\Delta P/P \ll 1$; 4) the radiative heat flux is constant while the turbulent heat flux increases; 5) the arc radius increases; 6) the electrical resistance from center to wall decreases exponentially; and 7) the stability radius (the equilibrium radius for stabilizing-destabilizing forces) increases until secondary injection occurs.

Nomenclature

A = cross-sectional area of constrictor, m^2
B = Planck function
E = voltage gradient, V/m
F = magnetic force, N/m^3
h = enthalpy, J/kg
I = current, A; radiant intensity, W/m^2
k = thermal conductivity, $W/m \cdot K$
ℓ = mixing length, m
m = mass flow rate, kg/s
P = Prandtl number; power, W
p = pressure, Pa
q = heat flux, W/m^2
r = radial distance from axis, m
s = ray path distance, m
S = swirl number, dimensionless
T = temperature, K
v = velocity, m/s
z = axial distance, m
ϵ = turbulent eddy viscosity, $N \cdot s/m^2$
ϕ = thermal potential, W/m
ρ = density, kg/m^3, torus major diameter, m
τ = shear stress, N/m^2; optical depth
η = electrical conductivity, S/m
μ = molecular viscosity, $N \cdot s/m^2$; radiation absorption coefficient, m^{-1}
θ = azimuthal coordinate, rad
σ = Stefan-Boltzmann constant

Subscripts

a = arc radius
e = equilibrium radius
k = kink
o = free space value; reference value
s = stability radius (normalized)
r = radial component; radiative component
z = axial value
w = wall value
t = total
tr = turbulent
c = conductive
θ = azimuthal component
ν = frequency
$+$ = positive going
$-$ = negative going

Presented as Paper 78-68 at the AIAA 16th Aerospace Sciences Meeting, Huntsville, Ala., Jan. 16-18, 1978; submitted Feb. 8, 1978; revision received June 6, 1978.

Index categories: Radiatively Coupled Flows and Heat Transfer; Thermal Modeling and Analysis; Plasma Dynamics and MHD.

*Scientist, McDonnell Douglas Research Laboratories. Member AIAA.

Introduction

THE electric arc heater (Fig. 1) provides required enthalpy-pressure environments for testing re-entry thermal protection systems and for nosetip material development and evaluation. Analytical modeling of arc heaters is required to determine the thermal and structural design of improved configurations, to project operating conditions for existing devices, to determine optimum locations and flow rates for secondary gas injection, and to provide stability analyses of new designs.

The need to consider swirl, turbulence, and radiation follows directly from the operational requirements of arc heaters used for thermal testing: gas swirl stabilizes the arc column,[1] turbulent modes of energy and momentum transfer result from the high mass flow rates (typically up to several kilograms per second), and radiation transport is dominant because of the high pressure (up to 25 MPa).

Although arc heater flowfields have been successfully modeled analytically,[2,3] the most successful prediction procedures used finite-difference methods for simultaneous solution of the fundamental conservation equations.[3] In a recent review of arc models, Incropera[3] concluded that, while approximate analytical models have suggested important trends, they have almost universally failed to quantify arc behavior accurately.

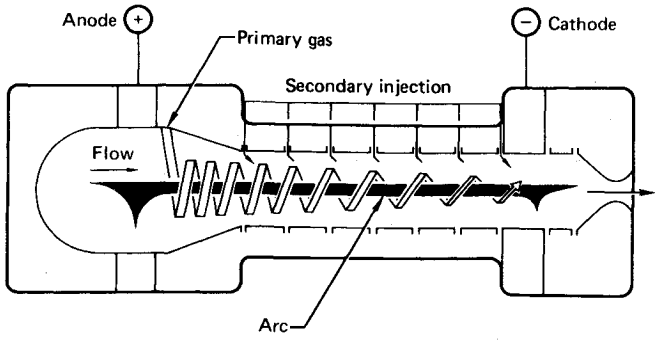

Fig. 1 Typical arc heater configuration.

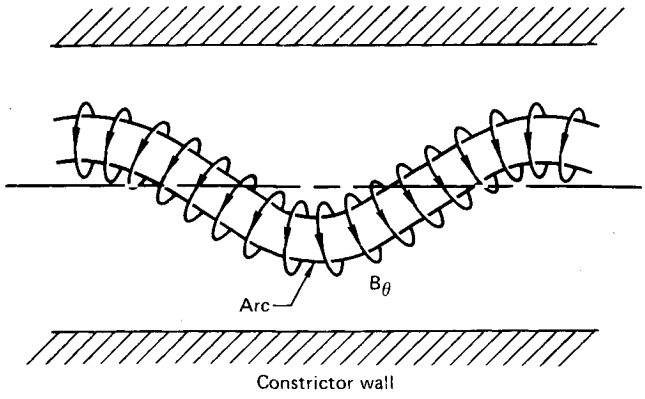

Fig. 2 Destabilizing kink forces.

General correlation procedures which relate the performance characteristics of a variety of heaters can be useful for predicting performance for small extrapolations from existing devices. Correlations, however, are not based on fundamental physical principles. They cannot confidently guide design efforts for new configurations and concepts, nor can they provide physical insight to evaluate existing devices.

Swirling gas flows stabilize confined electric arcs.[1] Swirl keeps the arc toward the center of the constrictor, away from the wall. The arc column is inherently unstable. When a slight bend in the arc occurs, the self-magnetic field on the inner portion of the bend increases, while that on the outer portion decreases (Fig. 2). This creates a net outward "kink" force which further distorts the arc toward the constrictor wall. If this kink is not opposed by a stabilizing force, such as a radial pressure gradient induced by gas swirl or externally imposed magnetic fields, the arc can shunt to the constrictor wall, affecting overall performance of the arc heater.

Previous numerical arc models, summarized in Table 1, have not simultaneously addressed the requirements of swirl, turbulence, and radiation. Furthermore, the problem of arc stability, as determined by comparing swirl and arc column kink forces, has not been addressed. The following model includes these features to characterize arc heater flowfields more completely.

Model

The present model, SWIRL ARC, is based on several assumptions which are used to isolate the dominate physical processes in the flowfield. These assumptions include:

1) Local thermodynamic equilibrium. Electron, ion and heavy-particle temperatures are considered equal for the high pressures considered. The single-fluid plasma model results.

2) Quasicylindrical assumption imposed (boundary-layer type). The radial velocities in the tube are much smaller than the axial or circumferential velocities, and the gradients in the radial direction are much stronger than those in the axial direction, $v_r \ll v_z \sim v_\theta$, $\partial/\partial r \gg \partial/\partial z$. The quasicylindrical conditions imply weak swirl (swirl number $S<1$); for strong swirl, reverse flow could exist where regions of $v_z=0$ would occur, violating the $v_z \gg v_r$ and $\partial/\partial r$ conditions.

3) Axial symmetry, $\partial/\partial\theta=0$.

4) Electric field is parallel to the constrictor axis and is constant along a radius.

5) Gas flow is steady in the mean, $\partial/\partial t=0$.

With the preceding assumptions, the model is summarized by the following set of time-averaged conservation equations in cylindrical coordinates using velocity components v_z, v_r, and v_θ; enthalpy h; and pressure p as the independent variables.

Energy

$$\rho v_z \frac{\partial h}{\partial z} + \rho v_r \frac{\partial h}{\partial r} = v_z \frac{\partial p}{\partial z} + v_r \frac{\partial p}{\partial r} + \eta E^2 - \frac{1}{r}\frac{\partial}{\partial r}(rq_r)$$

Axial Momentum

$$\rho v_z \frac{\partial v_z}{\partial z} + \rho v_r \frac{\partial v_z}{\partial r} = \frac{1}{r}\frac{\partial}{\partial r}(r\tau_{rz}) - \frac{\partial p}{\partial z}$$

Swirl Momentum

$$\rho v_z \frac{\partial v_\theta}{\partial z} + \rho v_r \frac{\partial v_\theta}{\partial r} + \rho \frac{v_r v_\theta}{r} = \frac{1}{r^2}\frac{\partial}{\partial r}(r^2 \tau_{r\theta})$$

Radial Momentum

$$\rho \frac{v_\theta^2}{r} = \frac{\partial p}{\partial r}$$

Continuity

$$\frac{\partial}{\partial z}(\rho v_z) + \frac{1}{r}\frac{\partial}{\partial r}(r\rho v_r) = 0$$

Table 1 Survey of arc heater numerical models

	Swirl	Shear model	Radiation model[a]	Gas	Secondary injection	Notes
SWIRL ARC	Yes	Turbulent	RT	Air, H_2/He	Yes	
Watson and Pegot[4]	No	Laminar	OT	N_2	Approximate	
Watson modified[5]	No	Turbulent	OT	N_2	Approximate	
ARCFLO II[6,7]	No	Turbulent	RT	Air, H_2/He	Approximate	
Bower I[8]	No	Laminar	OT	Argon	No	
Bower II[9,10]	No	Turbulent	OT	Argon	Yes	Explicit turbulence field model
Clark[11]	No	Laminar	OT	Argon	No	Nonequilibrium model
Graves and Wells[12]	No	Laminar and turbulent	OT	Air	No	
Walberg[13]	No	Laminar	RT	Air	No	Axial radiation transport
Neuberger[14,15]	Yes	Laminar	OT	N_2	No	

[a] OT = optically thin; RT = radiation transport (absorption model).

The electric field gradient, as a result of assumption 4, is

$$E = I \Big/ \int_0^{r_w} \eta \mathrm{d}A$$

The conductive heat flux q_c is expressed in terms of the thermal potential

$$q_c = -\frac{\partial \phi}{\partial r}$$

where ϕ is defined in terms of the thermal conductivity of the gas

$$\phi = \int_0^T k \mathrm{d}T$$

The turbulence model is based on Prandtl's mixing length theory, used in previous arc heater codes,[6] and on the assumption of isotropy for the $r-z$ and $r-\theta$ eddy viscosities[16]:

$$\tau_{rz} = (\epsilon + \mu)\frac{\partial v_z}{\partial r}, \quad \tau_{r\theta} = (\epsilon + \mu) r \frac{\partial}{\partial r}\left(\frac{v_\theta}{r}\right)$$

where μ is the molecular viscosity and ϵ is the turbulent apparent "eddy" viscosity. Isotropy sets $\epsilon = \epsilon_{rz} = \epsilon_{r\theta}$, and ϵ is then defined according to Lilley as[16]

$$\epsilon = \rho \ell^2 \left\{ \left(\frac{\partial v_z}{\partial r}\right)^2 + \left[r \frac{\partial}{\partial r}\left(\frac{v_\theta}{r}\right)\right]^2 \right\}^{1/2}$$

where the mixing length ℓ incorporates surface roughness.[6]

The turbulent heat flux q_{tr} is

$$q_{tr} = -\frac{\epsilon}{P_{tr}} \frac{\partial h}{\partial r}$$

where the turbulent Prandtl number is one recommended by Ref. 17.

The radiation heat flux is determined from a gray-gas emission-absorption model, similar to Ref. 6, so that absorption of radiation in the relatively cool outer-gas layers can be determined. The radiation heat flux vector, in accordance with previous assumptions, is radial, i.e., the radial temperature gradients are considered much greater than the axial gradients. The radiant intensity I_ν is obtained from the equation of radiant energy transfer for an absorbing and emitting gas in local thermodynamic equilibrium[18]:

$$-\frac{1}{\mu}\frac{\partial I_\nu}{\partial s} = I_\nu - B_\nu$$

where B_ν is the Planck function and μ is the absorption coefficient whose reciprocal can be interpreted as a mean-free path for photon absorption. With band-average absorption coefficients, B_ν can be replaced with $\sigma T^4/\pi$, where σ is the Stefan-Boltzmann constant. The variation of the absorption coefficient can be logarithmically interpolated[6] along a ray path between known radial mesh points j

$$\mu(s) = \mu(s_j)\left[\frac{\mu(s_{j+1})}{\mu(s_j)}\right]^{(s-s_j)/(s_{j+1}-s_j)}$$

which then yields the optical depth increment τ

$$\Delta\tau = \int_{s_j}^{s_{j+1}} \mu \mathrm{d}s = \frac{\mu_- \Delta s}{\ell n\,[\mu_+/\mu_-]}\left[\frac{\mu_+}{\mu_-} - 1\right]$$

and the positive and negative radiant intensities

$$I_+ = \int_{s_j}^{s_{j+1}} E e^{-\tau} \mathrm{d}\tau = \frac{\Delta s}{\Delta s - \ell n\,(E_+/E_-)}\left[E_- - E_+ e^{-B\Delta s}\right]$$

$$I_- = \frac{\Delta s}{\Delta s + \ell n\,(E_+/E_-)}\left[E_+ - E_- e^{-B\Delta s}\right]$$

where E is σT^4 and $B = 5/4$, which results from the exponential fit to the exponential integral fucntions peculiar to cylindrical geometry.[19-21] The net radiant heat flux is then found by summing the positive and negative rays

$$q_r = \sum_{n=1}^{N} (I_+ - I_-)\cos\gamma\Delta\gamma$$

where γ is the angle between the radiant flux I and the radius vector. The constrictor wall is assumed black, i.e., emission is equal to absorption $I_\nu\,(r_w) = B_\nu\,(r_w)$. For air the absorption coefficients are split into two bands, 0-10 eV and 10-100 eV.[6]

Swirl is characterized by the nondimensional swirl number S which is defined as the axial flow ratio of swirl to axial momentum[16]

$$S = \left(\int_0^{r_w} r\rho v_\theta v_z \mathrm{d}A\right) \Big/ \left(r_w \int_0^{r_w} \rho v_z^2 \mathrm{d}A\right)$$

The quasicylindrical approximation imposes a relatively weak swirl condition, $S<1$, where reverse flow does not occur and where flow angles at the wall are not much greater than 45 deg. This assumption causes the partial-differential equations to be parabolic in character, hence enabling a forward-marching solution.

Secondary gas injection at the constrictor wall, to augment the arc stabilizing swirl flowfield and/or sheath the constrictor wall with cold gas, is modeled by changing the wall boundary conditions for the radial and swirl velocity components from zero to a finite value (which was not done in Ref. 6). The wall swirl velocity is set to its maximum at the inlet, while the radial wall velocity is determined from the amount of secondary gas injection $\Delta\dot{m}$,

$$v_{r,w} = \Delta\dot{m}/2\pi\rho_w r_w \Delta_z$$

where ρ_w is the wall gas density based on the wall pressure and enthalpy. Nonzero radial and tangential wall velocities, the mathematical equivalent of source terms, model the addition of cold gas at the wall through the radial convection terms of the conservation equations.

The model equations are a coupled set of nonlinear, partial-differential parabolic equations which are solved numerically using an explicit finite-difference technique. The solution is a forward-axial-marching process starting from the inlet ($z=0$) with a prescribed wall pressure and a set of initial profiles for

Table 2 Sample case parameters[a]

Constrictor length	1.3 m
Arc current	700 A
Arc length	1.0 m
Constrictor diameter	254 mm
Initial conditions	
Swirl No.	0.7
Wall pressure	10 MPa (100 atm)
Mass flow	150 g/s (inlet)
Wall sandgrain roughness	0.127 mm
Total mass flow	200 g/s
Secondary mass flow	25% of total added from 0.5-1.0 m

[a] This case includes a constrictor length longer than the arc and secondary mass injection of 25%.

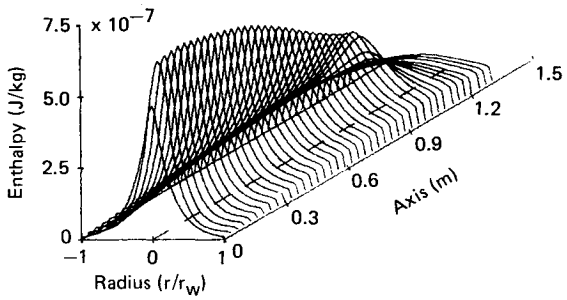

Fig. 3 Enthalpy profile.

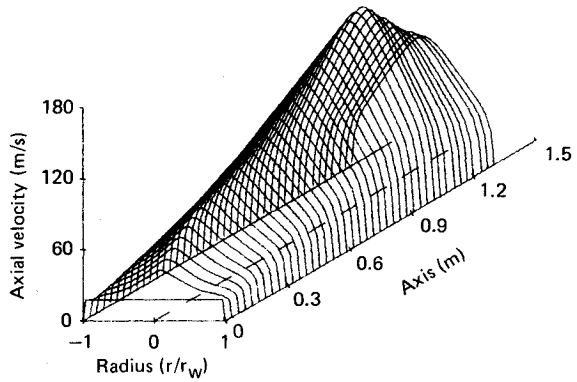

Fig. 4 Axial velocity profile.

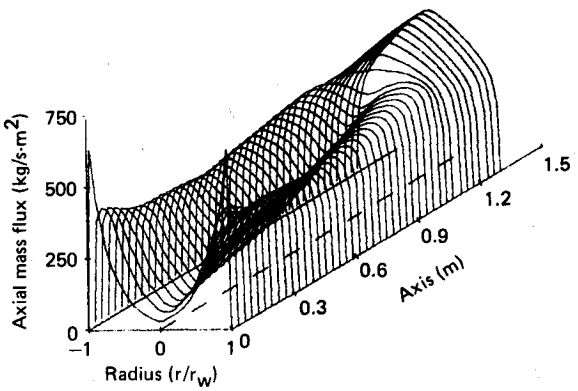

Fig. 5 Axial mass flux profile.

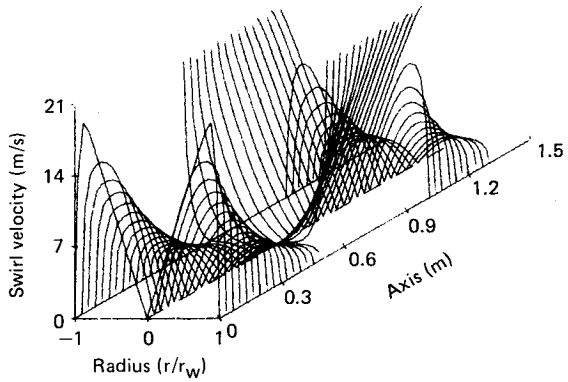

Fig. 6 Swirl velocity profile.

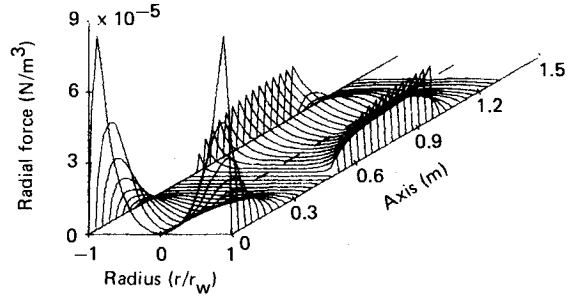

Fig. 7 Radial force profile.

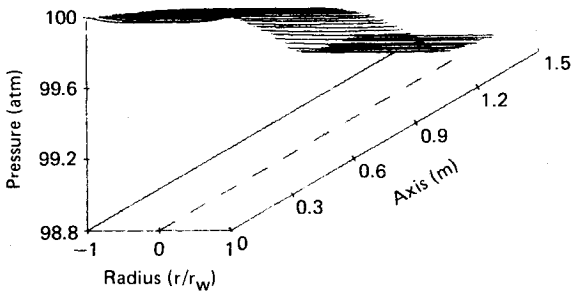

Fig. 8 Pressure profile.

enthalpy, axial velocity, and swirl velocity. The amplitudes of the p, v_z, and v_θ initial profiles are determined by the inlet values for the mass flow rate, the swirl number, the wall pressure, and the inlet enthalpy profile.

A provision was included in the code to delete the energy source term ("turn off" the arc current) so that relaxation of the energy flowfield can be predicted, i.e., mixing of the hot core gases and the resultant radial profiles downstream of the arc termination are calculated. This feature allows calculation of the enthalpy peaking ratio (the ratio of centerline to bulk average enthalpy) after the arc has terminated. The thermodynamic and transport properties for air are from Ref. 6 and for hydrogen-helium mixture ratios of 80:20, 50:50 and 20:80 are from Ref. 22.

Results

The results of a sample calculation for air are presented in Figs. 3-13 for the case outlined in Table 2.

Enthalpy field characteristics illustrated in Fig. 3 include the high-temperature arc represented by the peaked core, growth of the outer portions of the flow as the total energy of the gas increases, decline of the centerline enthalpy as the gas is heated, increase of the current-carrying cross section, and rapid decay of the centerline values when the arc is terminated and the cross-sectional profile flattens.

The axial velocity flowfield, Fig. 4, develops rapidly from the inlet parallel flow profile, accelerating as the gas is heated. When the arc is terminated, the lack of input energy and consequent energy loss cause the gas to decelerate.

The axial mass flux profile (ρv_z), Fig. 5, shows the effect of the high-temperature core in terms of decreased centerline density. Most of the mass flux is initially carried in the outer portion of the flow. As the gas is heated, the radial density differences becomes smaller and the center velocities greater; hence the centerline mass flux increases. When the arc is terminated, eliminating the high-temperature core, the density profile tends to follow the velocity profile.

The swirl velocity field, Fig. 6, rapidly decays from the inlet values until secondary injection occurs. At this point v_θ has a finite wall value, and the general swirl flow is accelerated until secondary flow is terminated and deceleration occurs. The swirl mass flux (ρv_θ) decays more rapidly than the swirl velocity field because of decreasing density as the gas temperature increases.

The radial force field, $\partial p/\partial r = \rho v_\theta^2/r$, used to stabilize the arc is shown in Fig. 7. This force field decays rapidly, because of the swirl and gas density decay, until secondary injection augments the swirl field. The flow angle, defined as $\alpha = \tan^{-1}$

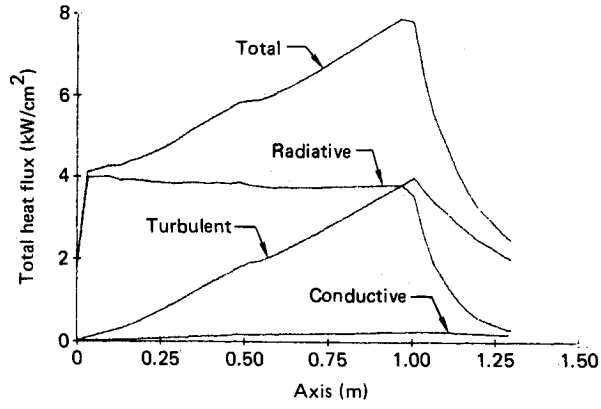

Fig. 9 Heat flux.

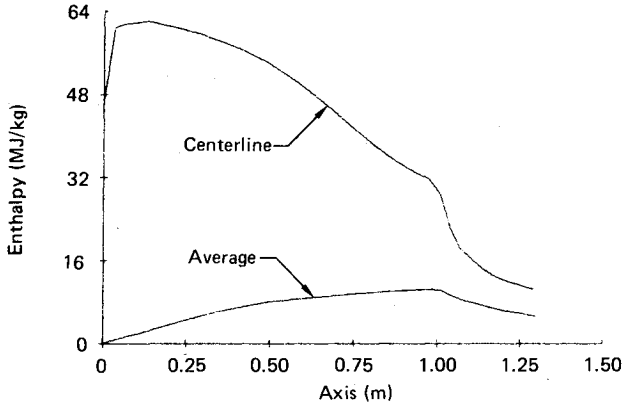

Fig. 10 Enthalpy.

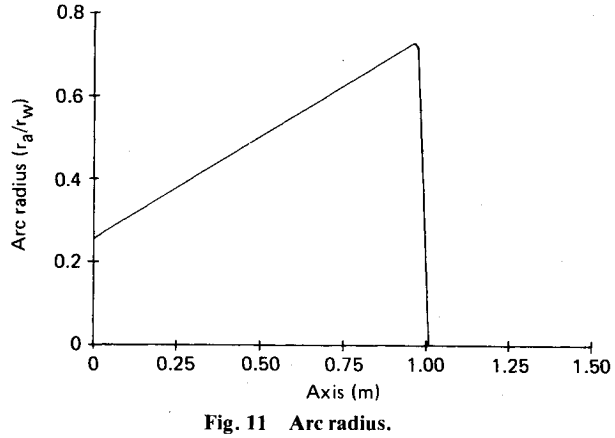

Fig. 11 Arc radius.

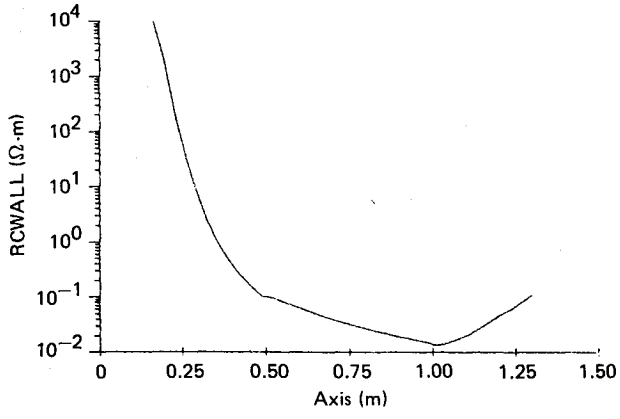

Fig. 12 RCWALL.

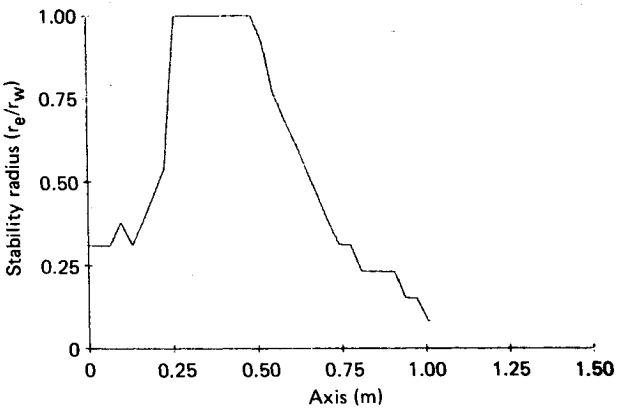

Fig. 13 Stability radius.

(v_θ/v_z), at the centerline is zero as dictated by the swirl profile and increases to a maximum near the wall. Flow angles decay with axial distance as the axial velocity field accelerates and the swirl velocity field decays. Secondary injection increases the flow angle.

The pressure field, shown in Fig. 8 on a magnified scale, indicates an axial pressure drop that is greater than the radial variation resulting from swirl. The relative radial pressure drop can be estimated independent of the code from the radial momentum equation

$$\frac{\partial p}{\partial r} = \frac{\rho v_\theta^2}{r} \rightarrow \frac{\Delta p}{p} \sim \frac{2\rho v_\theta^2}{p}$$

and with the estimate of $v_\theta \sim S v_z \sim S\dot{m}/\rho A$, so that

$$\frac{\Delta p}{p} = \frac{2}{p\rho}\left(\frac{S\dot{m}}{A}\right)^2$$

which for the present case is $\sim 10^{-4}$.

The resultant electric field gradient is relatively constant for a given mass flow. As the flow rate increases from secondary injection the gradient increases.

The total heat flux and its radiant, convective, and conductive components are shown in Fig. 9. The radiant contribution is relatively constant. The convective contribution increases as the net energy of the gas is increased. Secondary injection with cold gas at the wall causes only a slight change in the convective heat flux. The conductive heat flux is a minor contribution. When the arc is terminated, the radiant heat flux drops quickly, while the convective component decays at a slower rate.

The bulk enthalpy of the gas, Fig. 10, increases less rapidly in the secondary flow zone and decays after the arc is terminated. The centerline enthalpy, Fig. 10, decreases as the surrounding gas becomes heated. After arc termination, this value decreases as the high-temperature core relaxes. The power input to arc increases relatively linearly with axial distance.

The normalized radius of the arc column, defined as the radius in which 95% of the current is contained, is shown in Fig. 11. Note that at the inlet, the arc column is small, $r_a \sim 0.25\ r_w$, and grows steadily in cross section with a maximum diameter of $0.7\ r_w$ at termination.

The electrical resistance of the gas from the centerline to the wall is a measure of the electrical insulation properties of the gas between the arc and constrictor wall. It has been given the name RCWALL and is defined as

$$\text{RCWALL} = \int_0^{r_w} \frac{dr}{2\pi\eta}$$

Since the dimensions of RCWALL are (resistance)·(length), results must be divided by the axial length of interest to obtain a specific value. RCWALL is shown in Fig. 12 on a semilog plot, where values greater than 10^4 are suppressed to conserve cycles. The inlet values are greater than 10^4, illustrating the insulating properties of the outer sheath of cold gas. As the gas becomes heated, its resistance decreases exponentially. The effects of cold-gas secondary injection slows the rate at which RCWALL decreases. After the arc terminates and the gas temperature decreases, RCWALL increases slightly.

Stability

Stabilization in an arc heater is required to keep the arc column in a specified location, at a specified length, and terminated at each electrode where proper cooling techniques can be applied. Without stabilization, unwanted internal or external arc paths between the high-voltage electrodes can and do occur, causing disastrous consequences. Arc heaters for materials testing have generally been considered as vortex (swirl) stabilized or wall stabilized. With vortex stabilization, the constrictor wall is typically at ground potential, and the high-potential arc column is prevented from shorting to the wall by: 1) the electrical insulative properties of the cold outer gas sheath, and 2) keeping the small-diameter, unstable arc column from wandering near the wall. With wall stabilization, the constrictor wall is composed of many thin, electrically insulated segments such that each segment can float to the local arc column potential without disastrous effects. Thus, there is no requirement for cold insulative gas layers, or for keeping the arc column away from the wall. The penalty for this approach, however, is the complicated design and construction techniques for providing individual water cooling, for maintaining electrical insulation integrity, and insuring pressure vessel integrity.

These two types of stabilization have been considered mutually exclusive. The results of SWIRL ARC, however, indicate that these two approaches can be used in the same heater. In the entrance section of a heater, cold outer layers of gas can insulate the wall; the swirl forces are strong. As the gas becomes heated, the outer gas no longer insulates the wall, the arc diameter is a larger fraction of the constrictor diameter, and the swirl forces decay. Swirl stabilization is therefore ineffective, and wall stabilization must be used.

The second requirement for stabilization where there are cold outer insulative gas layers is the inward-directed radial force imparted by gas swirl. The arc in this region is typically an unstable filament, i.e., its diameter is small compared to r_w. The approach to defining arc column stability is to examine the balance between the gasdynamic forces and the arc column self-magnetic forces. This balance has been expressed mathematically by Schrade[23] as

$$\nabla \cdot (\rho \vec{v}\vec{v} + \vec{P}) = \vec{F}$$

where $\vec{F}$ is the magnetic force and is the divergence of the Maxwell stress tensor. If the balance of forces is not obtained for a radius less than the constrictor radius, then the arc column is not stabilized, i.e., the arc column kink forces are greater than pressure and inertia forces.

A practical engineering estimate of arc column stability can be obtained without a detailed time-dependent nonaxissymmetric solution of the preceding force relation by using its radial component, with the assumption that the inertia forces on the arc column are negligible because of the small values of gas density (resulting from the high arc column temperatures). With this approach, stability estimates can be made by comparing the radial pressure gradients, as calculated by SWIRL ARC, to the radially outward arc column kink force. Thus, the radius at which $\partial p/\partial r = F$ is the stability radius, r_e, where F is the outward radial force on the arc.

The estimate for the net force on a kinked current column (derived in the Appendix) is

$$F = \frac{\mu_0 I^2}{8\pi^2 r_a^2 r_k}$$

where I is the arc current, r_a the arc radius, μ_0 the permeability of free space, and r_k the radius of curvature of the kink. Note that when the current path is straight ($r_k = \infty$) the kink force goes to zero, indicating that this path is in unstable equilibrium.

The stabilizing radial pressure gradient, $\partial p/\partial r = \rho v_\theta^2/r$ (Fig. 7), is zero at the center and increases to a maximum near the wall. Thus, the swirl restricts the arc column from distorting beyond the equilibrium radius r_e. This radius, normalized to the constrictor wall radius, $r_e/r_w = r_s$, called the stability radius, has been computed in SWIRL ARC for the assumption that the worst-case kink radius is $r_k = r_w$. The results (Fig. 13) show that r_s, initially 0.3, quickly approaches unity, where swirl can no longer contain the arc from the wall because of the rapid decay of $\partial p/\partial r$, Fig. 7, as the swirl field and gas density decay. Secondary injection establishes the swirl flowfield again, and r_s becomes <1; the electrical insulation of the gas, however, is no longer present (Fig. 12); the ability of vortex stabilization to prevent arc shunting in this case is doubtful.

The swirl-induced stability is dependent upon 1) keeping the arc column from the wall, and 2) sufficient electrical insulation by the outer cooler gas to prevent electrical breakdown of the column to the wall. As the bulk gas becomes heated, swirl stabilization begins to fail because 1) electrical insulation is no longer present (RCWALL becomes small); 2) the arc radius grows to an appreciable fraction of the constrictor radius, making it more difficult to electrically isolate the arc from the wall; and 3) swirl forces decay. Thus, after the bulk gas has been heated sufficiently, wall stabilization must be utilized. The constrictor wall must be composed of electrically isolated segments where intimate contact between the arc column and the wall is not detrimental and the isolated constrictor segments are free to float to the arc column potential.

The preceding discussion and SWIRL ARC results support several recent arc heater design approaches by governmental[24,25] and industrial laboratories.[26] For example, a device for producing high core enthalpies without high-level bulk heating of the gas would have the following general characteristics: a small length-to-diameter ratio, a high-current, large-diameter arc and constrictor, swirl stabilization, and an arc termination as close to the model as practical, perhaps even with the arc terminated downstream of the supersonic nozzle. This approach uses the result that centerline enthalpy values do not decrease appreciably when the bulk gas is not heated. A device for uniformly heating the bulk gas to a high level would be characterized by a large length-to-diameter ratio with swirl stabilization and long segments used in the entrance region and wall stabilization with thin segments used in the more developed regions when

Table 3 Model comparisons[a]

Code	Enthalpy, MJ/kg	Voltage, V	Efficiency, %	Heat flux, kW/cm^2 q_r	q_c	q_{tr}
SWIRL ARC $S=0.5$	15.1	10 000	30.0	4.55	0.317	5.09
SWIRL ARC $S=0$	15.08	9 950	30.1	4.54	0.315	5.07
ARCFLO II[6,7]	15.6	9 190	34.2	4.96	0.327	3.06

[a] $I=800$ A; $p=10$ MPa (100 atm); $r_w=127$ mm; $\dot{m}=200$ g/s; surface roughness = 0.127 mm.

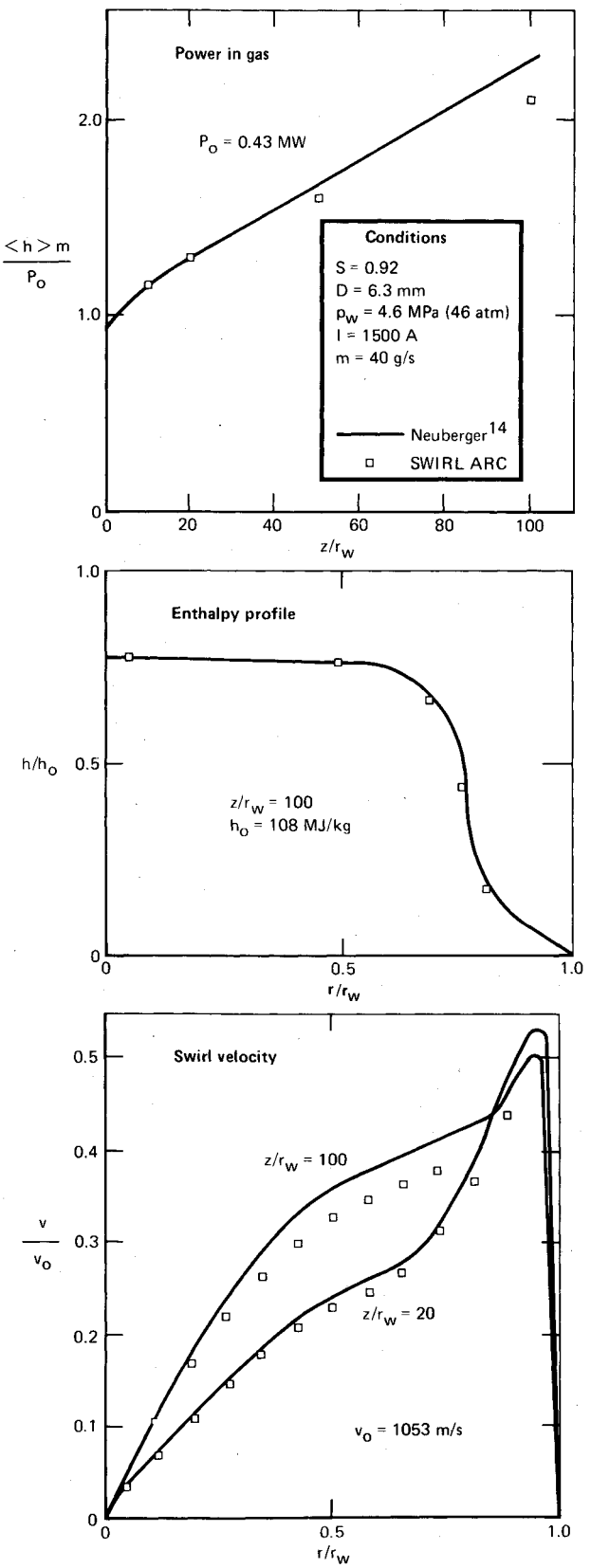

Fig. 14 Comparison of SWIRL ARC (with laminar model) to results of Neuberger.

the outer gas can no longer electrically isolate the wall from the arc.

Global Parameters

The predicted effects of swirl on the global parameters of voltage, average enthalpy, and heat flux are illustrated in

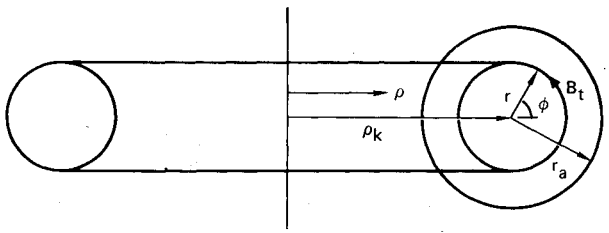

Fig. 15 Curved conductor (torus) coordinates.

Table 3 where the two SWIRL ARC cases differ only by the presence of swirl at the inlet. The results indicate that swirl does not appreciably affect the predicted global parameters of voltage, enthalpy, and heat flux. This is due to the relatively weak coupling between the swirl flowfield and the energy equation through the eddy viscosity and through the small radial pressure gradients. The swirl flowfield contributes to the eddy viscosity only near the wall where v_θ deviates from solid body rotation, $v_\theta \sim r$. As the gas becomes heated, the swirl field decays while the axial flow accelerates, decreasing the impact of swirl. The swirl-induced radial pressure differential is small; its influence on the thermodynamic and transport properties is neglibile. These results, of course, are predicated on the swirl condition, $S<1$. Swirl numbers of typical arc heaters at the inlet have not been measured; however, the arc track angles typically seen near the constrictor entrance are of the order of 45 deg, suggesting that if the arc foot follows the flow direction at the wall, the inlet swirl is less than one.

Since SWIRL ARC global predictions do not depend strongly on swirl, they can be validated indirectly by comparison with codes which do not contain swirl and which have been compared with experimental results.[6] Such a comparison is made in Table 3, and the results show reasonable agreement. Again this agreement is not surprising because, except for swirl, the two codes are based on approximately the same models and thermophysical properties. The improvements over Ref. 6 are the inclusion of the pressure term, Dp/Dt, in the energy equation, improved handling of secondary-injection wall-boundary conditions, second-order numerical wall derivatives, and an improved radiation computation; each of these parameters has a minor impact on the prediction of global parameters. The validation of the swirl portion of the predictions has been limited to comparison with the results of the Neuberger[14,15] swirl code for laminar flow with an optically thin radiation model; there is essentially agreement, as shown in Fig. 14.

Concluding Remarks

A model for swirling, turbulent, radiative flowfields in an arc heater typical of those used to produce ablative material test environments was developed, assuming that swirl-induced reverse flow does not occur ($S<1$) ($v_\theta \sim v_z \gg v_r$). Provisions for secondary injection with swirl were included, and the resulting time-averaged conservation equations were solved numerically.

The results of the model, applied to a representative high-pressure air arc heater, indicate (progressing axially, in the direction of the gas gaining energy) that: 1) the central enthalpy peak decreases; 2) the swirl flowfield and resultant stabilizing radial force decay rapidly until augmented by secondary wall injection; 3) the change in the radial pressure profile is small, $\Delta P/P \ll 1$; 4) the radiative heat flux is constant while the turbulent heat flux increases; 5) the arc radius increases; 6) the electrical resistance from center to wall decreases exponentially; and 7) the stability radius (the equilibrium radius for stabilizing-destabilizing forces) increases until secondary injection occurs.

Arc stability was discussed from two points of view; electrical isolation by cooler outer layers of gas combined with

arc column stabilization by swirl-induced radial forces, and by wall stabilization. An expression for the destabilizing arc kink force was obtained.

Appendix: Arc Column Kink Force Estimate

An electromagnetic force exists on an arc column which is curved. This force is due to the asymmetric interaction between the arc current and its self-magnetic field. A quantitative estimate of this force is required for comparisons with the radial pressure gradients for stability predictions. An expression for the local magnetic field about a curved conductor was required. The curved conductor was considered to be a local portion of a torus whose radius ρ_k corresponds to the kink radius of curvature. For a torus, Fig. 15, a body of revolution, the divergence of the magnetic field[27] is

$$\nabla \cdot \vec{B} = \frac{1}{\rho} \frac{\partial}{\partial t} (\rho B_t) = 0$$

which implies that away from the center, the magnetic field is $\sim \rho^{-1}$. The exact form for B_t, as a function of the distance r from the center of the arc, is found from the integral form of Ampere's law,

$$B_t = \frac{\mu_0 I r}{2\pi r_a^2} \frac{\rho_k \sqrt{1-(r/\rho_k)^2}}{\rho_k + r\cos\phi}$$

where ρ_k is the radius of curvature, r_a is the radius of the current column, and r is the distance from the center of current. The outward average force per unit volume is found by integrating the Lorentz force over the cross-sectional area

$$\langle F \rangle = \frac{1}{A} \int J B_t \cos\phi \, dA$$

The resulting average force, assuming uniform current density, is

$$\langle F \rangle = \frac{\mu_0 I^2}{8\pi^2 r_a^2 \rho_k} \left[1 + O\left(\frac{r_a}{\rho_k} \right)^2 \right]$$

Acknowledgment

The author is grateful to J. H. Painter for discussions, encouragement, and support, and for suggesting quantization of the RCWALL concept; to W. W. Bower for reviewing the arc model and for his helpful comments; and to J. M. Putnam for aid with the computer graphics. This research was conducted under the McDonnell Douglas Independent Research and Development Program.

References

[1] Traub, E., "Swirling Flows in Tubes and Their Application in the Stabilization of Electric Arcs," *Annalen Der Physik*, Vol. 18, 1933; translation FTD-HT-66-404, March 1967.

[2] Watson, V. R., "Comparison of Detailed Solutions with Simplified Theories for the Characteristics of the Constricted Arc Plasma Generator," *Heat Transfer and Fluid Mechanics Institute*, Los Angeles, Calif., June 1965.

[3] Incropera, F. P., "Procedures for Modeling Laminar Cascade Arc Behavior," *IEEE Transactions on Plasma Science*, PS-1, 1973.

[4] Watson, V. R. and Pegot, E. B., "Numerical Calculations for the Characteristics of a Gas Flowing Axially through a Constricted Arc," NASA TND-4042, June 1967.

[5] Watson, V. R., "Effects of Turbulence in Constricted Arc Plasma Generators," *Fifth NASA Intercenter and Contractor Conference on Plasma Physics*, Washington, D.C., May 1966.

[6] Nicolet, W. E., et al., "Analytical and Design Study for a High-Pressure High-Enthalpy Constricted Arc Heater," Arnold Engineering Development Center, Tenn., AEDC TR-75-47, July 1975.

[7] Nicolet, W. E., et al., "Methods for the Analysis of High-Pressure, High Enthalpy Constricted Arc Heater," AIAA Paper 75-704, 1975.

[8] Bower, W. W., "Correlations for the Wall Parameters in the Asymptotic Region of a Laminar Constricted Arc," M.S. Thesis, Purdue University, West Lafayette, Ind., June 1959.

[9] Bower, W. W., "A Model of Water and Transpiration Cooled Argon Constricted Arc Accounting for Turbulent Transport," Ph.D. Thesis, Purdue University, West Lafayette, Ind., June 1971.

[10] Bower, W. W., and Incopera, F. P., "A Procedure for Turbulent Arc Calculations," Aerospace Research Laboratories 73-0038, March 1973.

[11] Clark, K. J. and Incropera, F. P., "Thermochemical Nonequilibrium in an Argon Constricted Arc," AIAA Paper 71-593, 1971; also *AIAA Journal*, Vol. 10, Jan. 1972, pp. 17-18.

[12] Graves, R. A. and Wells, W. L., "Preliminary Study of a Wall-Stabilized Constricted Arc," NASA TMX-2700, Feb. 1973.

[13] Walberg, G. D., "Analysis of a Wall-Stabilized Arc Discharge with Three-Dimensional, Nongray Radiation Transport," Ph.D. Thesis, Dept. of Mechanical and Aerospace Engineering, North Carolina State University, Raleigh, N.C., 1974.

[14] Neuberger, A. W., "Heat Transfer in Swirling Compressible Plasma Flow," AIAA Paper 75-706, 1975.

[15] Neuberger, A. W., "Thermo-gasdynamical and Electrical Behavior of the Wall and Vortex-Stabilized Arc," Translation of DLR-FB-75-38, European Space Agency, ESA-TT-220, Dec. 1975.

[16] Lilley, D. G., "Prediction of Inert Turbulent Swirl Flows," *AIAA Journal*, Vol. 11, July 1973, pp. 955-960.

[17] Rotta, J. C., "Turbulent Boundary Layers in Incompressible Flow," *Progress in Aeronautical Sciences*, edited by A. Ferri, D. Kuchemann, and L. J. G. Sterne, Macmillan, New York, 1962, Vol. II.

[18] Vincenti, W. G. and Kruger, C. H., *Introduction to Physical Gas Dynamics*, Wiley, New York, 1965.

[19] Wessell, A. T. and Edwards, D. K., "Molecular Gas Band Radiation in Cylinders," *Journal of Heat Transfer*, Feb. 1974.

[20] Keston, A. S., "Radiant Heat Flux Distribution in a Cylindrically-Symmetric Non-isothermal Gas with Temperature-Dependent Absorption Coefficient," *Journal of Quantitative Spectroscopy and Radiative Transfer*, Vol. 8, 1968.

[21] Habib, I. S. and Greif, R., "Nongray Radiative Transport in a Cylindrical Medium," *Journal of Heat Transfer*, Feb. 1970.

[22] Clark, K. J., Nelson, E. V., Nicolet, W. E., Carlson, D. L., Balakrishnan, A., and Reese, J. J., Jr., "A Study of the Feasibility of Investigating Radiation/Turbulent Mixing-Layer-Interactions in a Constricted Arc," Aerotherm Final Rept. 75-167, Oct. 1975.

[23] Schrade, H. O., "The Momentum Equation to Describe the Dynamics of Electric Arcs," Aerospace Research Laboratories, ARL-72-0073, May 1972.

[24] Beachler, J. C., Kachel, W. A., and Cramer, K. R., "A New Arc Heater for Missile Nose Tip Testing," *Instrumentation in the Aerospace Industry*, Vol. 23; *Proceedings of the 23rd International Instrumentation Symposium*, Instrument Society of America, Las Vegas, Nev., May 1977.

[25] Horn, D. D. and Smith, R. T., "Results of Testing the AEDC 5-MW Segmented Arc Heater at Pressures up to 171 ATM," Arnold Engineering Development Center, Tenn., AEDC-TR-75-127, Nov. 1975.

[26] Painter, J. H., "Hybrid Arc Air Heater Performance," AIAA Paper 77-111, 1977.

[27] Mautz, J. R. and Harrington, R. F., "Radiation Scattering from Bodies of Revolution, *Applied Science Research*, Vol. 20, June 1969, pp. 405-435.